Accretion Disk Evolution With Wind Infall I. General Solution and Application to Sgr A*

Heino Falcke

Astronomy Department, University of Maryland, College Park, MD 20742-2421 (hfalcke@astro.umd.edu)

Fulvio Melia[1]

Department of Physics & Steward Observatory, University of Arizona, Tucson, AZ 85721 (melia@as.arizona.edu)

ABSTRACT

The evolution of an accretion disk can be influenced significantly by the deposition of mass and angular momentum by an infalling Bondi-Hoyle wind. Such a mass influx impacts the long-term behavior of the disk by providing additional sources of viscosity and heating. In this paper, we derive and solve the disk equations when these effects are taken into account. We present a survey of models with various wind configurations and demonstrate that the disk spectrum may then differ substantially from that of a standard α-disk. In particular, it is likely that a wind-fed disk has a significant infrared bump due to the deposition of energy in its outer region. We apply some of the results of our calculations to the Galactic Center black hole candidate Sgr A* and show that if a fossil disk is present in this source, it must have a very low viscosity parameter ($\alpha \lesssim 10^{-4}$) and the Bondi-Hoyle wind must be accreting with a very high specific angular momentum to prevent it from circularizing in the inner disk region where its impact would be most noticeable.

Subject headings: accretion, accretion disks, Bondi-Hoyle—black hole physics—Galaxy: center—Galaxy: Sgr A*

[1]Presidential Young Investigator

1. Introduction

1.1. Disk vs. Spherical Accretion

Compact objects, such as white dwarfs, neutron stars, and black holes may accrete either from the ambient medium (generally the Interstellar Medium — ISM) or from a companion in a binary configuration. Whether or not this accretion is mediated via a disk or it constitutes a more or less quasi-spherical infall depends critically on the specific angular momentum carried by the captured gas. It therefore is not always clear whether disk or quasi-spherical accretion dominates or if both are present.

For example, in Roche Lobe overflow, the gas circularizes quickly and forms a disk that can extend as far out as the binary orbital midpoint (e.g., Lamb & Melia 1987; Melia & Lamb 1987). Its temperature is generally too low to provide any significant support in the vertical direction, and so the disk is relatively flat and optically thick, at least until the gas approaches the inner regions close to the accreting object. Some binary systems are too wide for the companion to fill its Roche Lobe, and for these the accretion proceeds primarily via the capture of a portion of its wind by the compact object. In many circumstances, the latter's magnetic field is quite strong and the plasma is entrained onto its polar cap regions (e.g., Burnard, Klein & Arons 1988). Otherwise, the gas can either form a small (highly variable) disk whose size is specified by the circularization radius dictated by the specific angular momentum, or it may fall directly onto the accretor (Taam & Fryxell 1988).

In active galactic nuclei (AGN), the central, massive black hole generally accretes from the ambient medium. This can either be the ISM gas surrounding the nucleus or it may be the winds produced by stars in the central cluster. Although it is likely that Bondi-Hoyle accretion dominates the gaseous motions at large radii (out at the so-called accretion radius of order $0.1 - 1$ pc), there is ample evidence that much of the activity in AGNs is associated with an accretion disk at smaller radii. It appears, therefore, that the quasi-spherical accretion at large radii gradually settles into a planar, more or less Keplerian structure toward the central accretor, i.e., the accretion disk in these sources is 'fed' by the quasi-spherical infall.

1.2. Scope of the Paper

In this paper, we begin our study of the effects on the accretion disk evolution due to the continued infall from quasi-spherical accretion. We rederive the disk equations taking into account the contribution from the wind to the overall disk dissipation, the disk temperature, its column density, the accretion rate through the disk and the overall disk spectrum. All of these are expected to differ substantially between the isolated systems fed within a plane from their outer radii and those in which a disk is mainly fed from above.

The infalling gas can differ from the disk plasma in several respects: (i) its specific angular momentum at a given radius may be close to Keplerian (like that of the disk), or it may be much less, perhaps even zero, (ii) its mass flux may be much larger than that through the disk, and (iii) its ram pressure may differ significantly from that of the disk material, and thereby produce its own dynamical influence on the gas closer to the compact object.

We wish to study the impact of such a mass influx on the long-term behavior of the disk. In future work, we will couple this analysis with 3D hydrodynamic (and possibly magnetohydrodynamic) simulations of the ambient infall. This will provide much more realistic profiles of accreted mass and specific angular momentum as functions of radius in the disk. The process we discuss may be relevant to galactic nuclei as well as stellar mass black holes, neutron stars and star formation. Here we will concentrate on the former.

1.3. The Galactic Center

We shall specifically consider the example of the Galactic Center, where the presence of a supermassive black hole (coincident with the unique radio source Sgr A*) and strong, nearby stellar winds should lead to substantial Bondi-Hoyle accretion (e.g., Melia 1992; Ozernoy 1993; Ruffert & Melia 1994). In addition, stars may get tidally disrupted as they approach the strong central gravitational field. Depending on the strength of the disruption, as much as half of the stellar mass may be left as a remnant surrounding the black hole (Khohklov & Melia 1995 and references cited therein, particularly Rees 1990 and Shlossman, Begelman & Frank 1990). This remnant may, under some circumstances, form a relatively cold disk that evolves without a substantial mass infusion at its outer edge. Otherwise, there might also be a fossil accretion disk around the central black hole which is the remnant of a phase of higher activity in the past (Falcke & Heinrich 1994). In both cases the disk would inevitably interact with the infalling wind and thus change the matter inflow and the structure of the accretion disk. The resulting observational signature will then depend strongly on the ratio of wind to disk accretion rates, the viscosity in the disk, the specific angular momentum of the infalling matter and the time scales involved.

The broad-band radiative emission from Sgr A* may be produced either in the quasi-spherical accretion portion of the inflow (Melia 1992 & 1994) with $\dot{M}_{\rm w} \sim 10^{21-22}\,{\rm g\,s^{-1}}$, or by a combination of disk plus radio-jet (Falcke et al. 1993a&b; see Falcke 1996 for a review). As discussed above, quasi-spherical accretion seems to be unavoidable at large radii, but the low actual luminosity of Sgr A* seems to point to a much lower accretion rate in a starving disk and hence Sgr A* appears to be the ideal case for applying the concept of a fossil disk fed by quasi-spherical accretion. We note here that the disk may also be advective, in which case the luminosity may be decreased substantially due to the large fraction of dissipated energy carried inwards through the event horizon by the disk plasma (e.g., Narayan et al. 1995). In future developments of our model, we shall also consider such disk configurations.

The outline of the present paper is as follows: in Sec. 2 we discuss the wind energy deposition onto the disk and we will derive the equations for the evolution of an α-disk with arbitrary wind infall in Sec. 3; in Sec. 4 we will present numerical solutions for various parameters and discuss their implication for the Galactic Center in Section 5. The paper is summarized in Sec. 6, where we also describe further applications of our model.

2. Wind Energy Deposition Onto The Disk

When deriving the modified disk equations below, we will need to understand, at least crudely, the effects of the impacting wind on the disk, and where the energy is deposited. Since the inflow is usually highly supersonic near the surface of the disk (e.g., Coker et al. 1996, Paper II), it is reasonable to assume that the wind termination proceeds via a shock. To estimate the relevant time scales, we can make the rough approximation that an axisymmetric wind approaches the flat disk (of radius $R_{\rm d} = 10^{16}\,{\rm cm}\cdot R_{16}$) in free fall, with an accretion rate $\dot{M}_{\rm w} = 10^{-4} M_\odot \cdot \dot{M}_{-4}$. The black hole mass is taken to be $M_\bullet = 10^6\,M_\odot \cdot M_6$. As we shall see, these parameters are typical for weakly accreting nuclei, such as Sgr A* at the Galactic Center. For a strong shock, the downstream flow has a velocity

$$v_{\rm sh} \approx \frac{1}{4}\sqrt{\frac{2GM_\bullet}{R}} \approx 4\times10^7\,\frac{\rm cm}{\rm sec}\sqrt{\frac{M_6}{R_{16}}} \qquad (1)$$

and a density

$$n_{\rm sh} \approx \frac{\dot{M}_{\rm w}}{\pi R^2 v_{\rm sh} m_{\rm p}} \approx 3\times10^5\,{\rm cm}^{-3}\,\frac{\dot{M}_{-4}}{\sqrt{M_6 R_{16}^3}}, \qquad (2)$$

while the temperature of the shocked gas is given by

$$T_{\rm sh} = \frac{3 m_{\rm p} v_{\rm sh}^2}{k_{\rm B}} = 6\times10^7\,{\rm K}\,\frac{M_6}{R_{16}}. \qquad (3)$$

Behind the shock, the gas will have to settle onto the disk, which in our case is much cooler with a temperature $T_{\rm d}$ of several 100 to 1000 K. In this situation, the dominant radiative cooling mechanism of the hot shocked gas with energy density $dE/dV = 3/2 k_{\rm B} T_{\rm sh} n_{\rm sh}$ would be thermal Bremsstrahlung ($\epsilon_{\rm brems} = 1.7\times10^{-27}\ [T/{\rm K}]^{1/2}[n/{\rm cm}^{-3}]^2\,{\rm erg\,sec^{-1}cm^{-3}}$), corresponding to a cooling time scale of $t_{\rm brems} = 3\times 10^9\,{\rm sec}\ \ M_6 R_{16}/\dot{M}_{-4}$. By comparison, the subsonic flow time scale is $t_{\rm flow} = H_{\rm i}/v_{\rm sh}$, where $H_{\rm i}$ is the scale height of the shock above the disk. Thus, because

$$\frac{t_{\rm brems}}{t_{\rm w}} = 13\,\frac{M_6^{3/2}}{\dot{M}_{-4} R_{16}^{1/2}}\left(\frac{H_{\rm i}}{R}\right)^{-1} \qquad (4)$$

and $H_{\rm i} \ll R$, the gas cannot radiate appreciably before reaching the disk. If we express R in units of the gravitational radius, this ratio is inversely proportional to the Eddington luminosity of the black hole, and can become smaller than unity only for super-Eddington wind accretion or very large radii. In the post-shock region above the surface of the disk, the state of the gas is then almost always dictated solely by the influence of Coulomb scatterings and conductive heat transport.

Let the temperature, density, and height of this interface region between shock and disk be $T_{\rm i}$, $n_{\rm i}$, and $H_{\rm i}$, respectively, where $T_{\rm sh} > T_{\rm i} > T_{\rm d}$ and presumably $H_{\rm i} \ll R$ (see below). The density is given roughly by the balance of ram pressure and thermal (surface) pressure:

$$n_{\rm i} = 2.8 \times 10^{9}\,{\rm cm}^{-3}\,\frac{M_6^{1/2}\dot{M}_{-4}}{R_{16}^{5/2}}\left(\frac{T_{\rm i}}{1000\,{\rm K}}\right)^{-1}. \quad (5)$$

The conductive heat flux in the interface region is $q \sim 2.5 \times 10^{-6}\,{\rm erg/sec/cm}^2\ (T_{\rm i}/{\rm K})^{7/2}/(H_{\rm i}/{\rm cm})$ (Frank, King & Raine 1985, hereafter FKR, Eq. 3.42). It is not difficult to show that the ratio of the thermal conductivity time scale $t_{\rm con} = H_{\rm i} \cdot (dE/dV)/q$ to the flow time $t_{\rm i} = H_{\rm i}/v_{\rm sh}$ is

$$\frac{t_{\rm con}}{t_{\rm i}} \approx 0.35 \cdot \left(\frac{H_{\rm i}}{R}\right)\frac{\dot{M}_{-4}R_{16}^{3/2}}{M_6^{5/2}}\,, \quad (6)$$

which in most cases is much smaller than unity if $H_{\rm i} \ll R$, remains valid even for Eddingtion accretion and large radii, and is independent of the disk temperature.

An upper limit to the value of the scale height $H_{\rm i}$ is given by the Coulomb energy exchange length, based on the scattering time scale $t_{\rm coul} = 4.6 \times 10^{-25} v_{\rm sh}^5 n_{\rm i}^{-1} T_{\rm i}^{-1}\,{\rm K\,sec^6\,cm^{-8}}$ (FKR, Eq. 3.32) on which incoming particles share their energy with the background plasma. Since this time scale is extremely short, the wind/disk interface region is extremely thin (even compared to the disk scale height):

$$\frac{H_{\rm i}}{R} \lesssim 2 \times 10^{-6}\frac{\dot{M}_6^{5/2}}{\dot{M}_{-4}R_{16}^{3/2}}\,. \quad (7)$$

Thus, because of the high efficiency of thermal conduction and Coulomb scatterings, and the relatively large ram pressure, in almost all cases of interest most of the energy in the flow is deposited directly in a very thin layer onto the surface of the disk. Since the surface of the disk (in contrast to its interior) may be only weakly ionized, the incoming ions might actually penetrate somewhat below the disk surface until Coulomb interactions start to work and as $H_{\rm i}$ is so small, most of the energy will be deposited somewhere in or even beneath the surface layer. Given these conditions, we shall treat the disk as a large mass and heat sink for the inflowing wind. In particular, we shall assume for simplicity that the deposited energy is radiated as a (local) black body, since the spectral modifications due to bremsstrahlung emission above this region are expected to be small (see Eq. 4).

3. Modified Disk Equations

3.1. Mass and angular momentum conservation

The basic equations describing the evolution of an accretion disk are the mass conservation equation and the angular momentum equation (von Weizsäcker 1948; Lynden-Bell & Pringle 1974; see also Equations 5.3 and 5.4 in FKR). In the case of an accretion disk intercepting an external wind, these have to be modifed to include additional source terms from the external gas flow. If the wind produces a mass infall $\dot{\Sigma}_{\rm w}$(r,t) per unit area and time with a velocity $\vec{u} = (u_{\rm r}, u_\phi, u_{\rm z})$ in cylindrical coordinates, we obtain the mass equation

$$r\frac{\partial \Sigma}{\partial t} = -\frac{\partial}{\partial r}\left(r\Sigma v_{\rm r}\right) + r\dot{\Sigma}_{\rm w} \quad (8)$$

and the angular momentum equation

$$r\frac{\partial}{\partial t}\left(\Sigma r^2\omega\right) = -\frac{\partial}{\partial r}\left(r\Sigma v_{\rm r} r^2\omega\right) + \frac{1}{2\pi}\frac{\partial G}{\partial r} + r\dot{l}\,. \quad (9)$$

The other variables used here are the disk surface density Σ, the disk radius r, time t, (local) wind angular momentum flux $\dot{l} \equiv r\dot{\Sigma}_{\rm w}u_\phi$, disk internal viscous torque $G{=}2\pi r\nu\Sigma r^2\omega'$, partial radial derivative $' = \partial/\partial r$, internal disk viscosity ν, and the disk angular velocity $\omega{=}\sqrt{G_{\rm grav}M/r^3}$. Combining these equations yields

$$\frac{\partial \Sigma}{\partial t} = \frac{3}{r}\frac{\partial}{\partial r}\left[r^{1/2}\frac{\partial}{\partial r}\left(\nu\Sigma r^{1/2}\right) + \frac{2}{3}(1-\xi)^{-1}\nu_{\rm w}\Sigma\right] + \dot{\Sigma}_{\rm w}, \quad (10)$$

which is the well known partial differential equation for the time evolution of the surface density of the disk, but now including the effects of wind infall. The second equation, obtained by combining Equations 8 & 9, is the radial velocity of the accreting gas

$$v_{\rm r} = -\frac{3}{r\Sigma}\left[r^{1/2}\frac{\partial}{\partial r}\left(\nu\Sigma r^{1/2}\right) + \frac{2}{3}(1-\xi)^{-1}\nu_{\rm w}\Sigma\right]. \quad (11)$$

To permit a straightforward identification of the physical meaning of the new terms, and to provide a means of comparing the various effects in a simple manner, we define an external, rotational 'viscosity' $\nu_{\rm w}$ that describes the braking of the disk by the wind:

$$\nu_{\rm w} = (1-\xi)^2 r^2\frac{\dot{\Sigma}_{\rm w}}{\Sigma}, \quad (12)$$

and a parameter $\xi(r,t)$ that describes the angular velocity of the wind relative to its Keplerian value $v_\phi \equiv r\omega$, such that

$$u_\phi = \xi v_\phi \ . \tag{13}$$

For the type of accreted wind discussed in this paper, we have $-1 \le \xi \le 1$. The term $(1-\xi)^2$ in Equation 12 ensures that the viscosity is always positive even if the angular velocity of the external wind is larger than the Keplerian value. In the case of a wind flowing out from the center intercepting the disk with $\xi > 1$, the disk would be spun up and the radial disk inflow would be diminished by the external wind. This is reflected by a negative forefactor $(1-\xi)$ inside the brackets of Equations 10 & 11. The only disadvantage of this definition of $\nu_{\rm w}$ is the apparent singularity at $\xi = 1$, which, however, is not real as then also $\nu_{\rm w} = 0$.

In this definition we only consider the viscosity induced by the azimuthal velocity of the wind. The radial contributions of the momentum equation are neglected here but are considered in the energy equation as discussed below.

3.2. Energy equation

Any kind of viscosity, which is needed for the angular momentum and mass transport in the disk, is intimately linked to friction and dissipative processes. In accretion disk theory, it is usually assumed that the dissipated energy is radiated locally, though advection can under certain circumstances carry a significant fraction of the flux. The rate of energy dissipation is a function of the disk surface density, the viscosity and the shear rate. For the internal energy dissipation caused by turbulent viscosity and differential rotation in the disk, the rate of dissipated energy per unit area and time is (see FKR, Equation 4.25)

$$D_{\rm d} = \frac{1}{2}\,\nu\Sigma(r\omega')^2. \tag{14}$$

This is defined as dissipated energy per surface area and as we have 2 sides of the disk we get a factor of 1/2. Braking of the disk by the wind will cause a change in angular momentum, lead to friction between wind and disk and finally to energy dissipation. For now we will neglect the vertical structure of the disk and wind and treat the disk-wind interaction zone as an infinitesimally thin sheet in which the energy is dissipated (see Sec. 2 above). The dissipation rate, which is the change of energy ΔE per time Δt and surface area ΔA due to the friction between the wind and disk, can then be written as

$$\begin{aligned} D_{\rm w} &= \frac{1}{2}\,\frac{\Delta E}{\Delta t\ \Delta A} \\ &= \frac{1}{2}\,\frac{2\pi r(\Delta G_{\rm w}/r)}{\Delta t\ \Delta A} \\ &= \frac{1}{2}\,(v_\phi - u_\phi)^2\dot{\Sigma}_{\rm w} \ , \end{aligned} \tag{15}$$

using the torque

$$\Delta G_{\rm w} = r\dot{\Sigma}_{\rm w}(v_\phi - u_\phi)\Delta A \tag{16}$$

exerted by the infalling wind on the accretion disk on a time scale

$$\Delta t = 2\pi r/(v_\phi - u_\phi) \ , \tag{17}$$

given by the azimuthal velocity of the wind relative to the disk. Thus we obtain the final form for the dissipation rate and can express this in terms of the rotational viscosity $\nu_{\rm w}$ defined above:

$$\begin{aligned} D_{\rm w} &= (1/2)\,r^2\omega^2(1-\xi)^2\,(\dot{\Sigma}_{\rm w}/\Sigma)\,\Sigma \\ &= (1/2)\,\nu_{\rm w}\,\Sigma\,\omega^2 \ . \end{aligned} \tag{18}$$

Comparison of Equations 18 and 14 shows that our definition of $\nu_{\rm w}$ (Equation 12) is indeed justified.

In addition to the dissipative heating by rotational and turbulent friction we have to take the ram pressure of the wind into account, which results in a heating rate of a form similar to Equation 18. We shall consider both the $u_{\rm r}$ and $u_{\rm z}$ components of the wind ramming into the disk. It is assumed that the radial velocity of the disk is much smaller than the wind velocity $v_{\rm r} \ll \sqrt{u_{\rm r}^2 + u_{\rm z}^2}$ and that the radial pressure gradient induced by the wind is negligible for the disk structure. If all the kinetic energy associated with u_r and u_z is converted into heat and thus contributes to the total dissipation rate, we have an additional term

$$D_{\rm ram} = \frac{1}{2}\dot{\Sigma}_{\rm w}\left(v_{\rm r}^2 + v_{\rm z}^2\right) . \tag{19}$$

The total dissipation rate per surface area is then given by

$$D = D_{\rm d} + D_{\rm w} + D_{\rm ram}. \tag{20}$$

One should note that in any realistic case, the wind properties will be asymmetric with respect to the two sides of the disk: one would have to split Equations 18 and 19 accordingly and introduce separate parameters $\xi_{1|2}$, $\dot{\Sigma}_{\mathrm{w}1|2}$ and $\nu_{\mathrm{w}1|2}$ and obtain asymmetric dissipation rates. We do not want to introduce this complication into our model at the current stage.

3.3. The vertical structure

To solve the disk equations and obtain the evolution of Σ we need to know the radial dependence of the turbulent viscosity ν. This is usually done by introducing the Shakura & Sunyaev (1973) α parameter, defined such that

$$\nu = \alpha c_{\mathrm{s}} z_0 \ , \tag{21}$$

where c_{s} is the local sound speed, z_0 is the scale height of the disk and α is the dimensionless viscosity parameter, usually between 0 and 1. This has the benefit that the viscosity can be expressed in terms of local properties of the disk but has the disadvantage that one needs to solve its vertical structure.

The disk scale height can be obtained by demanding pressure equilibrium between internal gas pressure, gravitational attraction in the z-direction and external ram pressure from the wind. Substituting the gradient $\partial/\partial z$ with the scale height z_0, we obtain for a gas-pressure dominated disk with sound speed c_{s}

$$z_0 = \frac{c_{\mathrm{s}}}{\omega}\left(\sqrt{\left(\frac{1}{2}\frac{\dot{\Sigma}_{\mathrm{w}}}{\Sigma\omega}\frac{u_{\mathrm{z}}}{c_{\mathrm{s}}}\right)^2 + 1} - \frac{1}{2}\frac{\dot{\Sigma}_{\mathrm{w}}}{\Sigma\omega}\frac{u_{\mathrm{z}}}{c_{\mathrm{s}}}\right). \tag{22}$$

This means that the disk is substantially squeezed if $u_{\mathrm{z}}\dot{\Sigma}_{\mathrm{w}}/\Sigma \gg 2c_{\mathrm{s}}\omega$; if u_{z} is of the order of the Keplerian velocity (i.e., $u_{\mathrm{z}} \sim r\omega$) then we have the condition

$$2\Sigma/\dot{\Sigma}_{\mathrm{w}} \ll (c_{\mathrm{s}} r)^{-1} \tag{23}$$

for the time scale involved in order to compress the disk. The left hand side is the time scale of the wind interception and the right hand side the *global* thermal time scale of the disk.

To complete our set of basic equations, we need to specify the central temperature in the disk to get the sound speed. We assume that the energy dissipated by viscous processes *in the disk* diffuses outwards from the central plane by radiative energy transport in an optically thick medium (with optical depth $\tau \gg 1$) in local thermal equilibrium. This will give us an energy flux of dissipated energy in the disk at its surface of

$$F_{\mathrm{d}}(z_0) = D_{\mathrm{d}} = -\frac{4\sigma}{3}\frac{\Delta T(z_0)^4}{\Delta\tau}, \tag{24}$$

the Δ here signifying changes in the corresponding quantity between the disk's midplane and its surface. The total energy flux will then be the sum of the energy dissipated in the disk and the energy dissipated by the impact of the wind on the surface of the disk. If this is radiated immediately by black body radiation with an effective temperature T_{eff}, we have

$$F_{\mathrm{tot}}(z_0) = \sigma T_{\mathrm{eff}}(r,t)^4 = D(r,t), \tag{25}$$

and we can set $T(z_0) = T_{\mathrm{eff}}$. With $\Delta T \equiv T(z_0) - T(0)$ and $\Delta\tau \sim \tau$, we can solve Equation 24 for $T(0)$, getting

$$T(0)^4 = \frac{1}{\sigma}\left[\left(\frac{3\tau}{4}+1\right)D_{\mathrm{d}} + D_{\mathrm{w}} + D_{\mathrm{ram}}\right]. \tag{26}$$

This equation reduces to the usual equation for the central temperature if $D_{\mathrm{w}} \sim 0$, $D_{\mathrm{ram}} \sim 0$ and $\tau \gg 1$, but it also allows a situation where the dissipation is dominated completely by the impact of the wind. This will increase the central temperature and make the temperature gradient shallower and in the extreme case could lead to a quasi-isothermal disk; in the cases discussed in this paper, this does not happen.

With the central temperature at hand we can now evaluate the pressure

$$P = \frac{\rho k_{\mathrm{b}} T}{\mu m_{\mathrm{p}}} \tag{27}$$

and the sound speed

$$c_{\mathrm{s}} = \sqrt{P/\rho}, \tag{28}$$

if we solve the second order partial differential equation for $\partial\Sigma/\partial t$ (Equation 10). We only need to specify the opacity. Assuming that we are in the outer and cooler region of the disk, we may consider simply the contribution from free-free absorption which gives us

$$\kappa = 6.6\cdot 10^{22}\mathrm{cm}^2/\mathrm{g}\left(\frac{\rho}{1\ \mathrm{g/cm}^3}\right)\left(\frac{T}{1\ \mathrm{K}}\right)^{-7/2}. \tag{29}$$

This opacity will become progressively less accurate as we move to very cold or very hot disks, but we ignore this trend here, since we are primarily interested in a basic understanding of the disk evolution and the main effects. We hope to include a more elaborate opacity function for more realistic calculations in a future version.

The complete set of equations can now be solved numerically. For each time step we calculate the radial gradients in Σ on the right-hand side of Equation 10 to get $\partial\Sigma/\partial t$ and an estimate for Σ at the next time step using a simple Runge-Kutta algorithm with adaptive step size. The vertical structure has to be calculated at every step and because the height is no longer a simple function of $c_{\rm s}$ and ω, we have to solve this set of equations implicitly. Fortunately, $c_{\rm s}$ changes only slowly so one can use the sound speed from the previous step as a first guess and achieve convergence very quickly.

3.4. Spectrum

To get a rough spectrum from the accretion disk, we have integrated black body spectra with the local effective temperature $T_{\rm eff}(r)$ over the entire disk surface. Following our discussion in Sec. 2, we consider $T_{\rm eff}$ to represent the total dissipation rate, as indicated in Equations 20 & 25. Here, we have neglected all vertical transport processes that might modify the disk spectrum. Mainly because of the difficulties in comparing disk spectra to observations and the uncertainties involved in the vertical disk structure itself, the theory for radiation transport in disk atmospheres is not well developed, especially in the case of AGN disks. While Sun & Malkan (1989) find that the pure black body integration can explain AGN spectra sufficiently well, Laor & Netzer (1989) have used a simplified treatment to account for the effects of the vertical structure. The changes to the calculated spectrum are, however, so small, especially compared to the scarce data for the Galactic Center, that inclusion of these effects would neither be opportune nor testable. For simplicity we also calculate our spectra for only one inclination angle $i = 60°$ (i.e. $\cos i = 0.5$). The spectra we show should therefore be considered only as a first order approximation and one should bear in mind that orientation effects, relativistic effects, limb-darkening, and propagation effects will lead to a somewhat different appearace.

4. Numerical Solutions

As an example of the evolution of a disk with wind infall, we choose parameters that might roughly be appropriate for the Galactic Center, i.e. a black hole mass of $M_\bullet = 10^6 M_\odot$, an accretion rate for the fossil disk of $\dot{M}_0 = 10^{-8} M_\odot/{\rm yr}$, a wind infall rate of $\dot{M}_{\rm w} = 10^{-4} M_\odot/{\rm yr}$, and an α of 10^{-4} (e.g. Falcke & Heinrich 1994). For simplicity in this first series of tests, we will correlate the vertical wind velocity directly to its radial velocity, such that

$$u_{\rm z} = \sqrt{1-\xi^2}\, v_\phi \quad \text{and} \quad u_{\rm r} = 0. \tag{30}$$

The boundary conditions for the innermost ring of the disk ($r_{\rm in} = 6R_{\rm g} \equiv 6G_{\rm grav}M_\bullet/c^2$) are such that we impose $\partial\Sigma/\partial t = 0$ and $\Sigma = 0$ to account for the presence of the black hole. The outer boundary (at $r = r_{\rm out}$) can be free (using only the one-sided derivative) or be fixed to a certain $\dot{M}(r_{\rm out})$ by virtue of Equation 11 and $\dot{M}(r) = -2\pi r v_{\rm r}\Sigma$, thus setting the square bracket in Equation 10 to $\dot{M}(r_{\rm out})/6\pi$ at $r = r_{\rm out}$. The radial velocity is also limited to not exceed the free-fall velocity. Even though we are here discussing the situation pertaining to a black hole, we ignore any relativistic effects, which are not critical as long as the wind affects mainly the outer portions of the disk. During the calculations we check that the total mass in the system is indeed conserved.

4.1. Validation of the code

To validate our code and test its reliability, we first calculate the disk evolution in two scenarios without wind infall to compare the surface density profiles with those of the stationary solution.

Empty Disk We start with an almost empty, very low Σ disk and feed it with a very high accretion rate close to the Eddington value of $\dot{M} = 10^{-2} M_\odot/{\rm yr}$ at $r_{\rm out}$ until an equilibrium state is reached. Figure 1 shows how the accreted matter quickly fills the almost empty disk and then slowly approaches the analytical Shakura & Sunyaev solution for the steady state (upper panel in Fig. 1). Also, $\dot{M}$ approaches a constant value for all r.

Gaussian Ring In a second test, a textbook example, we start with a ring with a Gaussian surface density distribution in r and no accretion from the outer boundary. Figure 2 shows that the ring evolves towards the stationary solution with constant $\dot{M}$. In the outer regions, matter is actually flowing out, carrying away the angular momentum; only there one can see a deviation from the stationary solution. In the later evolution (not shown here), the disk runs out of fuel with a decreasing surface density and size but it retains its basic shape.

The agreement between the analytical and numerical solutions demonstrates that our code produces reliable results.

4.2. Disk evolution with a large scale wind

In the first scenario where we allow a wind to fall onto the disk we assume that the disk intercepts the inflow over a fairly large region, extending out to a radius $r = 90000 R_{\rm g} \simeq 10^{16}$cm. In the absence of detailed hydrodynamical simulations, we do not yet know what the radial distribution of the wind is and we here consider the case of a constant mass infall per unit area, which means that the impact of the wind is felt most strongly at the largest radii, but is still present in the inner regions. More realistic distributions will be discussed in the second paper, where we will use the results of numerical 3D wind calculations.

Maximum Angular Momentum Figure 3 shows the evolution of a fossil disk intercepting a wind with constant $\dot{\Sigma}_{\rm w}$ over a large collecting area, as described in the previous paragraph. Hence, the largest fraction of the wind is intercepted at large radii, which leads to a significant increase of the surface density there. Because the viscous time scale (starting with the assumed $\alpha = 10^{-4}$) is too long for a radial transport of the matter — the viscosity increases only by a factor of three during the simulation — the modest increase in Σ at smaller radii is due mostly to the local wind infall. After many time steps, the pile-up in the outer disk starts to become less pronounced due to radial accretion and the entire disk begins to converge towards the stationary solution. The time scale for an increase in surface density and luminosity is larger than about 10^6 yrs. We note that the dynamical time scale (~ 20 years) for the disk calculated from its rotation velocity is 10^5 times shorter than the time scale for the disk structure to change in response to the wind. Hence, the most notable change is expected to be the spectrum. The wind infall leads to a local increase in the disk accretion rate and the production of an infrared (IR) bump — the spectrum becomes almost flat.

Hurricane If we simulate a "hurricane" (Fig. 4), where all the mass is deposited within an annulus (bound by the radii $30000 - 90000\ R_{\rm g}$), the mass piles up in the outer region with a gradual transfer toward smaller radii over a 10^8-yr time scale. Again, this reflects the large viscous time scale in the disk assuming that $\alpha = 10^{-4}$ remains constant over this period, and is similar to the 'empty disk' scenario discussed above.

Zero Angular Momentum The time scale for the transfer of mass inwards toward smaller radii shortens dramatically when the infalling wind carries sub-Keplerian angular momentum. The importance of the variations in angular momentum and velocity distributions in the wind is highlighted in Figure 5, where we have repeated the previous calculation (shown in Fig. 3) for a free-falling wind with zero angular momentum ($\xi = 0$). The IR bump jumps almost immediately to the value that corresponds to the high accretion rate in the wind. The reason for this is that the non-zero vertical impact velocity of the wind and the strong friction between wind and disk lead to a rapid dissipation of energy and rapid radial accretion. The deposition of mass with zero angular momentum in the disk also leads to a compression of the disk in the radial direction (the outer rings move inwards as they become sub-Keplerian) and results in an increase in surface density beyond the value induced by the increased mass deposition through the wind alone. Also the viscosity increases much more strongly.

4.3. Disk evolution with a small scale wind

In some systems, the wind flowing into the inner disk region may carry very little specific angular momentum. In this case, because the circularization radius can be significantly smaller than the fossil disk's outer radius, the impact of the infalling gas on some portions of the disk can be much larger because the wind is now restricted to a smaller disk surface area and hence accounts for a significantly larger local flow rate. We have therefore repeated the above calculations, but now with a reduced interception region designated by a radius 100 times smaller than used in the previous section. This leads to a much stronger effect on the disk because of the higher $\dot{\Sigma}_{\rm w}$ and the correspondingly shorter time scales.

Maximum Angular Momentum For a wind with the local Keplerian velocity (Fig. 6), the disk reacts almost immediately at all radii because the wind infall dominates the radial accretion rate everywhere. Still, the infall is more prominent in the outer region in the beginning, yielding an almost radially constant surface density. As soon as the viscous mass transport has caught up, the surface density profile approaches the *stationary solution*. The mass transport at the outer wind radius is bi-directional, like in the gaussian density distribution (Sec. 4.1), so that beyond the wind accretion radius matter is flowing outwards and not inwards. The spectrum is immediately dominated by emission from the outer region because the kinetic energy of the wind (in u_z) is dissipated immediately, but since the interaction region of the disk is so small, we do not see two bumps. After viscous processes have transported the higher accretion rate inwards, the spectrum simply broadens somewhat towards higher frequencies.

Zero Angular Momentum The situation becomes even more extreme if the wind has no angular momentum. Within ~ 1000 years (which is still much longer than the dynamical time scale) the incorporated mass in the outer region becomes equal to the stored mass in the disk. Because of the low angular momentum, the mass falls into a lower orbit within this short period of time, leaving a gap behind until the fossilized angular momentum in the disk stops a further free fall. The accretion flow is now purely inwards and after it is stabilized continues to grow on a longer time scale (10^5 yrs). The spectrum is immediately dominated by a single Planck-spectrum from the outer region.

5. Preliminary Application To Sgr A*

5.1. The basic scenario

As our first (and necessarily simplified) application of the results in the previous section, we now consider the situation in the Galactic Center. There exists ample evidence for the presence of a strong wind in the region around Sgr A*, with a characteristic velocity $v_w \sim 500 - 700$ km s^{-1} and mass loss rate $\dot{M}_w \sim 10^{-3}\ M_\odot$ yr^{-1} (see Melia 1994 and the references cited therein, particularly Hall, Kleinmann & Scoville 1982, Geballe et al. 1991, Krabbe et al. 1991 and Gatley et al. 1986, among others). In addition, the latest stellar kinematic studies point to a likely mass of $M \approx 1.8\ (\pm 0.5) \times 10^6\ M_\odot$ for the central object (Haller et al. 1995), and so it is expected that Sgr A* is accreting at a rate of about $10^{(-5)\text{ to }(-4)} M_\odot$/yr (Ruffert & Melia 1994) via Bondi-Hoyle accretion.

However, the luminosity of Sgr A* is tightly constrained to a value of a few $10^5 L_\odot$ (Falcke et al. 1993a; Zylka et al. 1995). Thus, if the accretion flow eventually turns into a disk at smaller radii, and assuming a conversion efficiency of about 10% rest mass energy into radiation, we infer a disk accretion rate of a few $10^{-7} M_\odot$/yr. If the winds surrounding the central black hole are relatively uniform, the fluctuations in the accreted specific angular momentum are sufficiently small that only a small (less than about $5 - 10$ Schwarzschild radii in size) disk is then expected to form (Melia 1994; Ruffert & Melia 1994). Such a small disk could be consistent with the low luminosity observed from this region, but it is likely that gradients in the ambient medium produce a bigger specific angular momentum in the accreted material, and hence a larger circularization radius. This could be due in part to the fact that the Galactic Center wind is comprised of several stellar components, which would make the flow around Sgr A* nonuniform. Departures from uniformity increase the accreted specific angular momentum since the cancellations in the post bow-shock flow are not complete — one side tends to dominate over the other, producing a net accreted angular momentum. The correspondingly larger circularization radius produces a bigger and presumably brighter disk. Another way of saying this is that the infalling gas from a non-uniform medium retains a larger Keplerian energy that must be dissipated as it drifts inwards toward the black hole.

It could be that the disk, if large, is highly advective (Narayan et al. 1995). The role of advection has usually been ignored in α-disk theory, but several studies (e.g., by Abramowitz et al. 1988, 1995, and more recently by Narayan & Yi 1994) have shown that under some circumstances, the internal disk energy can constitute a substantial radial flux when it is transported by the inward drift. As much as 90% or more of the locally dissipated gravitational energy flux can be carried away in this manner, thereby decreasing the radiated luminosity for a given mass accretion rate by as much as an order of magnitude, and possibly more. However, without detailed radiative-hydrodynamical simulations, this scenario is at best still only a possibility.

It has also been suggested that Sgr A* might be surrounded by a large, slowly accreting, fossil disk, perhaps formed from the remnants of a tidally-disrupted star that ventured too close to the black hole. In this case one expects that the large-scale Bondi-Hoyle inflow must then be captured and incorporated into the disk. The latter might remain faint if most of the quasi-spherical infall circularizes at large radii, for the incorporated gas would require a fairly long viscous time scale in order to reach the central black hole and produce the correspondingly high luminosity output (Falcke & Heinrich 1994). A fossil disk could also act as a resevoir for the infalling plasma, thereby delaying the dissipation of its energy.

5.2. Model vs. observation

Many of the calculations reported in this paper correspond to a situation similar to that of Sgr A*. In order for a particular model to be relevant to this source, it should be able to account for the high wind-accretion rate and yet a low luminosity of a few $10^5 L_\odot$. Recent NIR observations of Sgr A* appear to show 5 different sources within the Sgr A* error box (Eckart et al. 1995), though the source separation in this image is smaller than the telescope's diffraction limit. If this separation of the infrared emission from this region is real, the limit on Sgr A*'s luminosity could be as low as $L_\nu < 3 \cdot 10^{21}$ erg/sec/Hz (for an interstellar absorption of $A_K = 3.7$) in the K-band ($\sim 10^{14}$ Hz). The upper limit for Sgr A* at 12.4μm ($10^{13.4}$ Hz) is 0.1 Jy ($0.9 \cdot 10^{22}$ erg/sec/Hz) (Gezari et al. 1996). Recently Stolovy, Hayward, & Herter (1996) claimed a detection of Sgr A* at 8.7μm (100 mJy dereddened) which may be interesting with respect to our work but needs further confirmation. A starving accretion disk with $\dot{M} < 10^{-8} M_\odot$/yr, as used in our simulations, could be consistent with those numbers when the following additional factors are taken into account. Requiring that the disk is seen edge-on ($\cos\theta \lesssim 0.1$), would reduce the flux displayed in the figures by another factor 5. Moreover, there are indications that Sgr A* is intrinsically absorbed (Predehl & Trümper 1994) — in addition to the interstellar attenuation — which would reduce the observed luminosity further.

A second important factor to take into account when comparing particular models to the observations is the time scale required for a change in the radial accretion rate. If the main components in the Bondi-Hoyle accretion are the stellar winds of central He I stars, the accreting medium should have been there a certain fraction of the stars' lifetime ($\sim 3 - 7 \times 10^6$ years, Krabbe et al. 1995), though probably not longer than this. We would therefore expect that a typical time scale for the accretion process should be longer than of order a million years if a fossil disk is involved.

The luminosity and time scale constraints would therefore seem to rule out situations in which the wind is captured by the disk at small radii, because they produce spectra that are too luminous in the NIR and IR very quickly after the onset of Bondi-Hoyle accretion (Figs. 6 & 7). In other words, the post-bow shock flow cannot be carrying a small specific angular momentum (which would lead to circularization at small radii), but rather should have sufficient azimuthal velocity to allow it to merge with the fossil disk near its outer edge. However, models with a low angular momentum wind that is captured far out in the disk fare no better (as far as Sgr A* is concerned; see Fig. 5) because they violate the IR limits due to their instant transformation of kinetic energy into heat and thence into IR radiation.

It appears from our analysis of the calculations that the only class of models that might be consistent with the observations of Sgr A* are those in which the angular momentum of the wind is large enough that the infall circularizes at a radius $\gtrsim 10^{16}$ cm and settles gently onto the disk (Figs. 3 & 4). In addition, the α-parameter must be small ($\alpha \ll 1$) in order to prolong the transfer of the deposited wind material into the center. The 'hurricane' model with $\alpha \lesssim 10^{-4}$ seems to be a viable scenario, though this model does not even require the presence of a fossil accretion disk to stop the infall because the high angular momentum wind will circularize and stop at larger radii anyway. If it exists, a starving, fossil disk may even lie closer to the black hole and not be coupled directly with the large scale disk formed by the wind infall.

6. Discussion

In this paper we have rederived the basic equations for an α-accretion disk with the consideration of wind infall. Besides a source term for the mass, the wind infall also introduces a dynamical viscosity $\nu_{\rm w}$ to the basic equations when its angular momentum is sub-Keplerian. We have calculated the evolution of an accretion disk with wind infall for various sets of parameters, leading to some interesting effects not present in conventional accretion disk theory. The situation we considered in detail is that of a fossil accretion disk, which intercepts a wind with a much higher accretion rate than the former. As long as the viscosity parameter in such a disk is very small ($\alpha \ll 1$), the time during which the surface density of the disk changes is much longer than the dynamical time scale because of its large mass storage capability. In this case, the disk is not blown away and it can incorporate winds with very high mass accretion rates. A large, non-coaxial angular momentum in the wind may, however, lead to a warping of the disk which we ignore here.

The overall evolution of the disk may be described in terms of two basic classical solutions: (a) that of an almost empty disk that is fed from the outside and (b) an initial ring of matter that evolves with time and where most of the matter is flowing in, while a small fraction flows outwards carrying away the angular momentum. If the intercepted wind has a low specific angular momentum, the disk will shrink in the radial direction on a short time scale determined by $\Sigma/\dot{\Sigma}_{\rm w}$ and de-couple from its outer region, forming a gap. The matter piles up until viscous processes in the disk become important and the inner regions are filled up like in the empty disk evolution. For a high specific angular momentum wind, the disk will also have a radial outflow in its outer portion like in the ring evolution. The interaction between wind and disk leads to an additional heating of the disk on its surface and a moderate increase in the viscosity and therefore a faster evolution; the effect is stronger for a sub-Keplerian wind.

The most important changes with respect to the conventional solutions concern the emitted spectrum: the emission at lower-frequencies is enhanced. This may produce either a flattening of the spectrum or even a strong low-frequency bump (in AGN the bump would be produced in the IR). This bump can be as luminous as the primary bump produced in the inner region of the disk or even brighter. The most drastic effect is due to the angular momentum deposited by the wind. When the wind has a Keplerian velocity and settles gently onto the disk ($u_{\rm z} = 0$), the formation of the low-frequency bump may take a long time $\Sigma/\dot{\Sigma}_{\rm w}$, while a wind with a low specific angular momentum and a high $u_{\rm z}$ will release its kinetic energy very quickly and the low-frequency bump will appear almost instantaneously. In both cases, however, it will take a viscous time R^2/ν for the increased accretion rate in the outer part to reach the inner region and lead to an increase of the (usually dominating) high-frequency emission.

The process described here has many potential applications. The production of an IR bump by an infalling wind, perhaps from the nuclear star cluster or a circumnuclear starburst, would be an interesting — although as yet undeveloped — signature to investigate. A scenario such as this can also be invoked to account for some observational characteristics in winds onto protostellar disks. In this paper, we have briefly discussed the application of our model to the Galactic Center source Sgr A*.

The presence of strong stellar winds and a high central mass concentration in the Galactic Center appear to be inconsistent with the low Infrared luminosity of the putative supermassive black hole, Sgr A*. We have considered the possibility that this object may be surrounded by a fossil disk accreting at a rate of $10^{-8} M_\odot$/yr, while it is intercepting the incoming wind with $\dot{M}_{\rm w} \lesssim 10^{-4} M_\odot$/yr. Current observational limits for Sgr A* are very restrictive and we have found that they are not consistent with most of the wind specific angular momentum configurations we have considered here. As the estimates for the bolometric luminosity of Sgr A* may change, the direct observations in the IR and NIR are the most critical limits to be observed in this respect and we find that any fossil disk would become too luminous too quickly in those bands. We can only reconcile the data with the models if the wind circularizes on a scale of $\gtrsim 10^{16}$ cm and if the α-parameter within the disk is $\lesssim 10^{-4}$. Without detailed numerical simulations, these numbers are at best only estimates. Even so, it seems safe to conclude that if a fossil disk is present around Sgr A*, then it must have a very low α and the wind must carry a large specific angular momentum in order to describe Sgr A* self-consistently. This rules out a large region of the phase space available for possible models of Sgr A*.

In a future extension of this work, we plan to couple our calculations to 3D hydrodynamical simulations for the large scale Bondi-Hoyle accretion (Paper II) in order to get a better estimate for the radial distribution of the wind infall. As we have seen here, the specific angular momentum of the wind appears to be the most critical parameter. Further improvements of our model will include a more accurate description of the opacity and the possible warping of the disk by a very strong, asymmetric wind.

This research was supported in part by the NSF under grant PHY 88-57218, and by NASA under grants NAGW-2518 and NAG8-1027.

REFERENCES

Abramowicz, M.A., Chen, X., Kato, S., Lasota, J. P., & Regev, O. 1995, Ap.J. Letters, 438, L37

Abramowicz, M.A., Czerny, B., Lasota, J. P., & Szuskeiwicz, E. 1988, Ap.J., 332, 646

Burnard, D.J., Klein, R.I. & Arons, J. 1988, Ap.J., 324, 1001

Coker, R., Melia, F., Falcke, H. 1996, in prep. (Paper II)

Eckart, A., Genzel, R., Hofmann, R., Sams, B.J., & Tacconi-Garman, L.E. 1995, ApJ 445, L23

Falcke, H. 1996, in "Unsolved Problems of the Milky Way", IAU Symp. 169, L. Blitz & Teuben P.J. (eds.), Kluwer, Dordrecht, p. 163

Falcke, H., Biermann, P. L., Duschl, W. J., & Mezger, P. G. 1993a, A&A 270, 102

Falcke, H., Mannheim, K., & Biermann, P. L. 1993b, A&A 278, L1

Falcke, H., & Biermann, P.L. 1995, A&A 293, 665

Falcke, H., & Heinrich, O. 1994, A&A 292, 430

Frank, J., King, A.R., & Raine, D.J. 1985, "Accretion Power in Astrophysics", Cambridge University Press (FKR)

Gatley, I., Jones, T.J., Hyland, A.R., Wade, R., Geballe, T.R, and Krisciumas, K. 1986, MNRAS, 222, 562

Geballe, T.R., Krisciunas, K., Bailey, J.A., Wade, R. 1991, Ap.J. Letters, 370, L73

Gezari, D., Dwek, E., & Varosi, F. 1996, in "Unsolved Problems of the Milky Way", IAU Symp. 169, L. Blitz & Teuben P.J. (eds.), Kluwer, Dordrecht, p. 263

Hall, D.N.B., Kleinmann, S.G. and Scoville, N.Z. 1982, Ap.J. Letters, 260, L63

Haller J., Rieke, M., Rieke, G., Tamblyn, P. Close, L. & Melia, F. 1995, Ap.J., in press

Krabbe, A., Genzel, R., Drapatz, S., and Rotaciuc, V. 1991, Ap.J. Letters, in press

Krabbe, A., Genzel, R., Eckart, A. et al. 1995, ApJ 447, L95

Lamb, D.Q. & Melia, F. 1987, Ap.J. Letters, 321, L133

Laor, A., & Netzer, H. 1989, MNRAS 238, 897

Lynden-Bell, D., & Pringle, J. E. 1974, MNRAS 168, 603

Melia, F. 1992, ApJ 387, L25

Melia, F. 1994, ApJ 426, 677

Melia, F. & Lamb, D.Q. 1987, Ap.J. Letters, 321, L139

Narayan, R. & Yi, I. 1994, Ap.J. Letters, 428, L13

Narayan, R., Yi, I., & Mahadevan, R. 1995, Nature 374, 623

Ozernoy, L. 1992, "Back to the Galaxy", AIP Conf. Ser. 254, S.S. Holt et al. (eds.), New York, p. 40,44

Predehl, P., & Trümper, J. 1994, A&A 290, L29

Rees, M.J. 1990, Science, 247, 817

Ruffert, M., & Melia, F. 1994, A&A 288, L29

Shakura, N.I., & Sunyaev, R.A. 1973, A&A 24, 337

Shlossman, I., Begelman, M.C. & Frank, J. 1990, Nature, 345, 679

Stolovy S.R., Hawyard T., Herter T. 1996, ApJ Letters, in press

Sun, W.H., Malkan, M.A. 1989, ApJ 346, 68

Taam, R.E. & Fryxell, B.A. 1988, Ap.J. Letters, 327, L73

von Weizsäcker, C.F., 1948, Zeitschrift f. Naturf. 3 a, 524

Zylka, R., Mezger, P.G., Ward-Thomson, D., Duschl, W., & Lesch, H. 1995, A&A 297, 83

This 2-column preprint was prepared with the AAS LATEX macros v4.0.

Fig. 1.— Surface density evolution of an almost empty disk that is fed from the outer boundary with $10^{-2} M_{\odot}/\mathrm{yr}$. The analytical stationary solution is given by the dashed-dotted line. The lower panel (the zero Σ distribution is outside the plot range here) shows the evolution on an extended time scale compared to the upper panel.

Fig. 2.— Surface density and accretion rate evolution of a Gaussian ring with no external feeding. For comparison, two appropriately scaled stationary solutions are plotted, the upper curve corresponding to $\dot{M} = 10^{-2}\ M_{\odot}/\mathrm{yr}$ and the lower one to an accretion rate roughly 5 times lower, which is the actual accretion rate in the disk.

Fig. 3.— Surface density and emitted spectrum evolution of a fossil accretion disk with strong wind deposition; the wind has Keplerian azimuthal velocity ($M_{\bullet} = 10^{6} M_{\odot}$, $\dot{M}_0 = 10^{-8} M_{\odot}/\mathrm{yr}$, $\alpha = 10^{-4}$, $\dot{M}_{\mathrm{w}} = 10^{-4} M_{\odot}/\mathrm{yr}$, $\xi = 1$, and $r_{\mathrm{w}} = 90000 R_{\mathrm{g}}$).

Fig. 4.— Surface density and emitted spectrum evolution of a fossil accretion disk with strong wind deposition only within the outer ring (a "hurricane"); the wind has Keplerian azimuthal velocity ($M_{\bullet} = 10^{6} M_{\odot}$, $\dot{M}_0 = 10^{-8} M_{\odot}/\mathrm{yr}$, $\alpha = 10^{-4}$, $\dot{M}_{\mathrm{w}} = 10^{-4} M_{\odot}/\mathrm{yr}$, $\xi = 1$, and $r_{\mathrm{w}} = 30000 - 90000 R_{\mathrm{g}}$).

Fig. 5.— Surface density and emitted spectrum evolution of a fossil accretion disk with strong wind deposition; the wind has zero azimuthal velocity ($M_{\bullet} = 10^{6} M_{\odot}$, $\dot{M}_0 = 10^{-8} M_{\odot}/\mathrm{yr}$, $\alpha = 10^{-4}$, $\dot{M}_{\mathrm{w}} = 10^{-4} M_{\odot}/\mathrm{yr}$, $\xi = 0$, and $r_{\mathrm{w}} = 90000 R_{\mathrm{g}}$).

Fig. 6.— Surface density, emitted spectrum, and accretion rate evolution of a fossil accretion disk with strong wind deposition at small radii; the wind has a Keplerian azimuthal velocity ($M_{\bullet} = 10^{6} M_{\odot}$, $\dot{M}_0 = 10^{-8} M_{\odot}/\mathrm{yr}$, $\alpha = 10^{-4}$, $\dot{M}_{\mathrm{w}} = 10^{-4} M_{\odot}/\mathrm{yr}$, $\xi = 1$, and $r_{\mathrm{w}} = 900 R_{\mathrm{g}}$). For comparison we have plotted a stationary solution on top of the Σ curves (dashed-dotted line, top figure).

Fig. 7.— Surface density, emitted spectrum, and accretion rate evolution of a fossil accretion disk with strong wind deposition at small radii; the wind has zero angular momentum ($M_{\bullet} = 10^{6} M_{\odot}$, $\dot{M}_0 = 10^{-8} M_{\odot}/\mathrm{yr}$, $\alpha = 10^{-4}$, $\dot{M}_{\mathrm{w}} = 10^{-4} M_{\odot}/\mathrm{yr}$, $\xi = 0$, and $r_{\mathrm{w}} = 900 R_{\mathrm{g}}$). For comparison we have plotted a stationary solution on top of the Σ curves (dashed-dotted line, top figure). The height in the 'gap' is an artifact, as there is no disk anymore in this region.

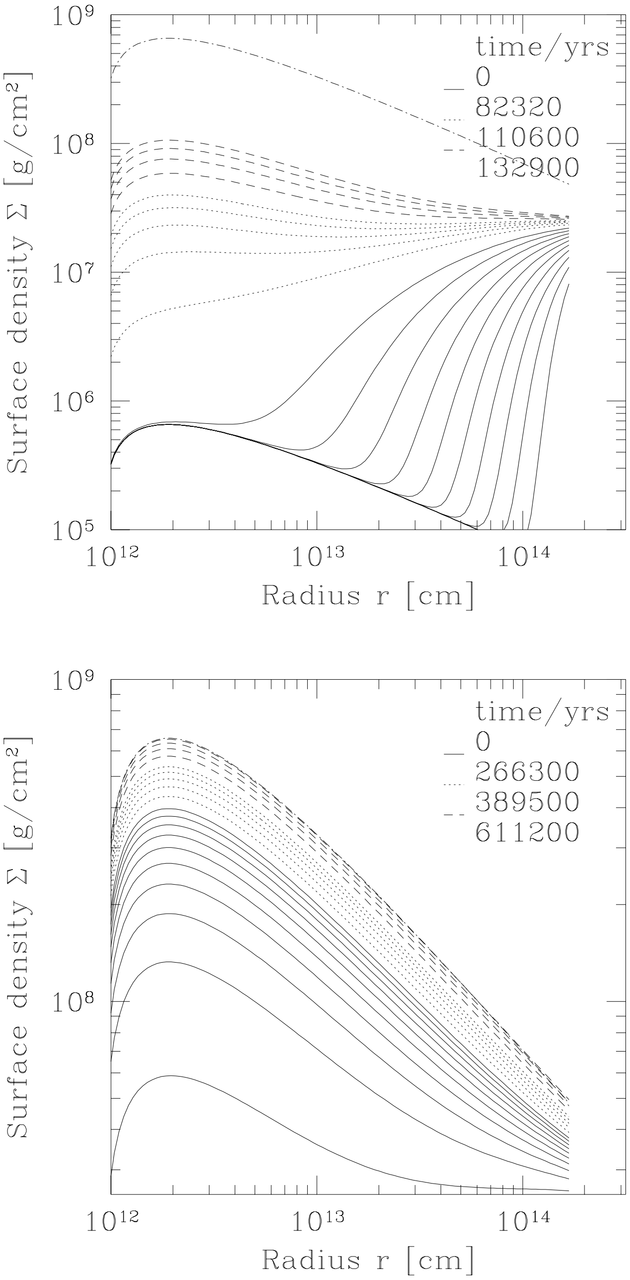

time/yrs
0
82320
110600
132900
Surface density Σ [g/cm²]
Radius r [cm]
time/yrs
0
266300
389500
611200
Surface density Σ [g/cm²]
Radius r [cm]

Figure 1

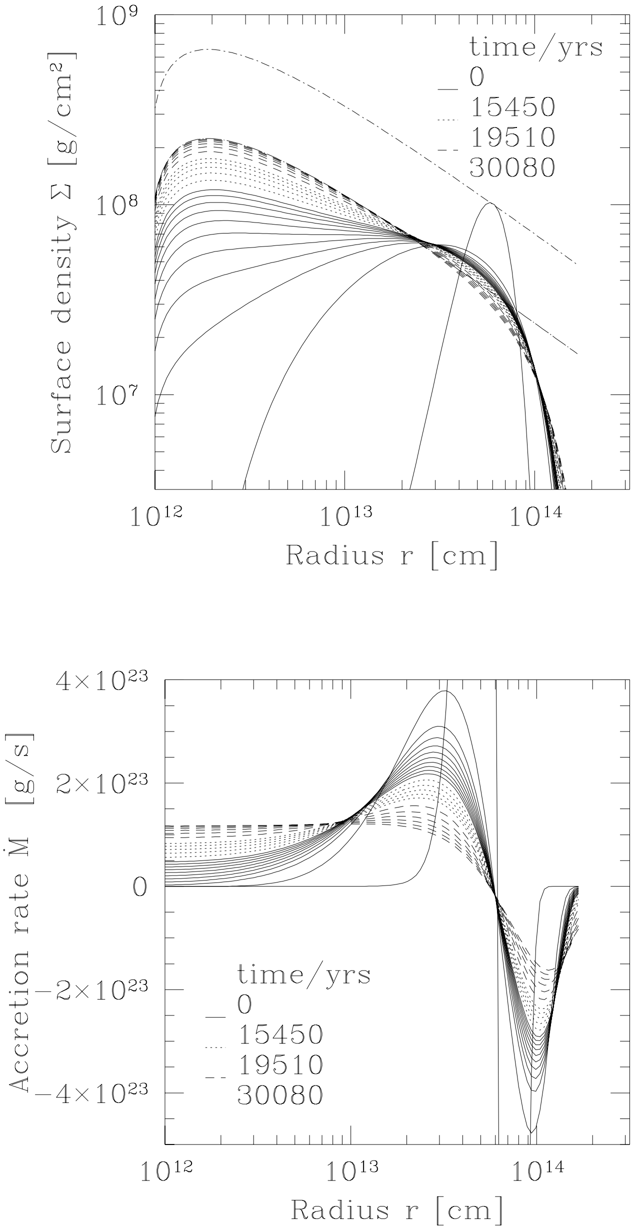
time/yrs
0
15450
19510
30080
Surface density Σ [g/cm²]
Radius r [cm]
10^{9}
10^{8}
10^{7}
10^{12}
10^{13}
10^{14}
Accretion rate Ṁ [g/s]
4×10^{23}
2×10^{23}
0
-2×10^{23}
-4×10^{23}

Figure 2

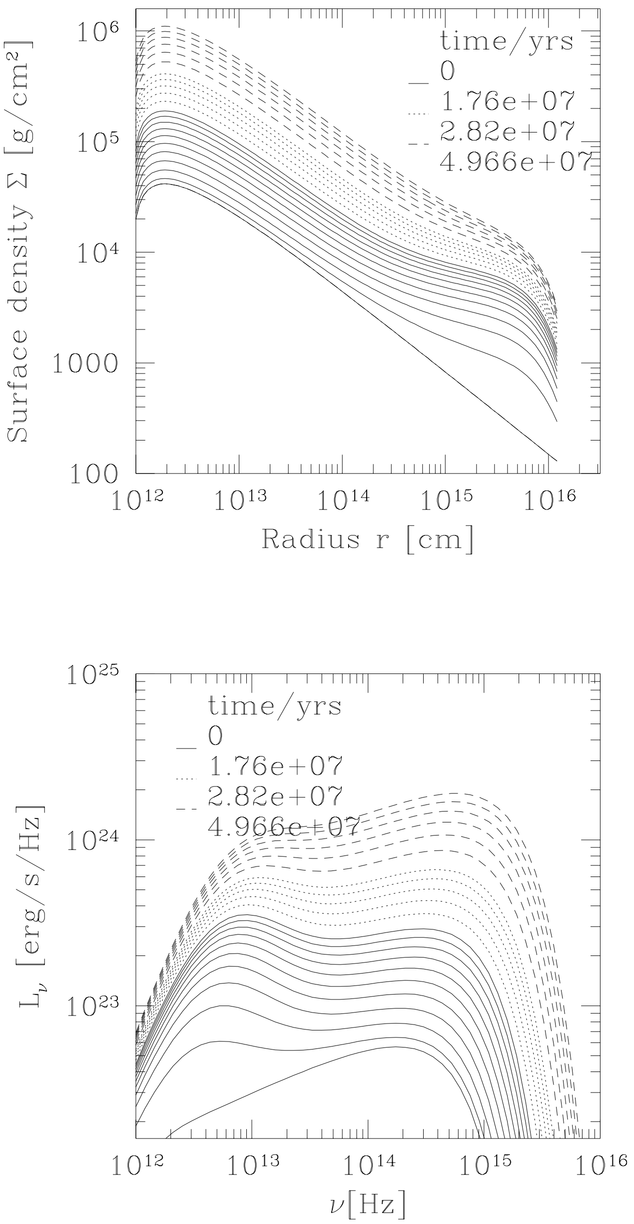
time/yrs
0
1.76e+07
2.82e+07
4.966e+07
Surface density Σ [g/cm²]
100
1000
10^4
10^5
10^6
10^{12}
10^{13}
10^{14}
10^{15}
10^{16}
Radius r [cm]
time/yrs
0
1.76e+07
2.82e+07
4.966e+07
L_ν [erg/s/Hz]
10^{23}
10^{24}
10^{25}
10^{12}
10^{13}
10^{14}
10^{15}
10^{16}
ν[Hz]

Figure 3

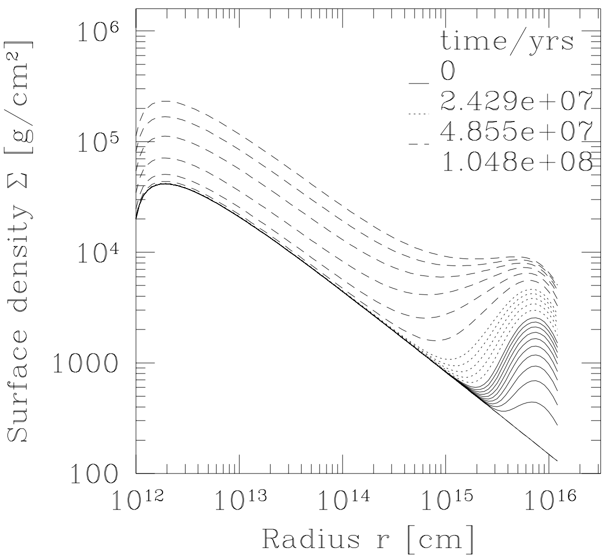

time/yrs
0
2.429e+07
4.855e+07
1.048e+08
Surface density Σ [g/cm²]
10^6
10^5
10^4
1000
100
10^{12}
10^{13}
10^{14}
10^{15}
10^{16}
Radius r [cm]

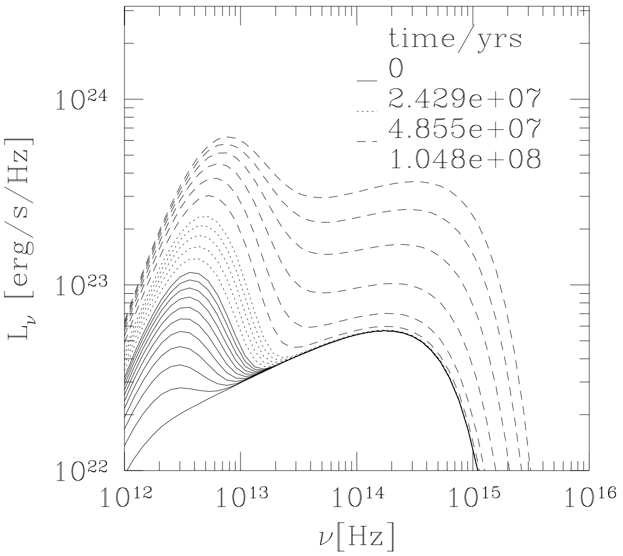

time/yrs
0
2.429e+07
4.855e+07
1.048e+08
L_ν [erg/s/Hz]
10^{24}
10^{23}
10^{22}
10^{12}
10^{13}
10^{14}
10^{15}
10^{16}
ν[Hz]

Figure 4

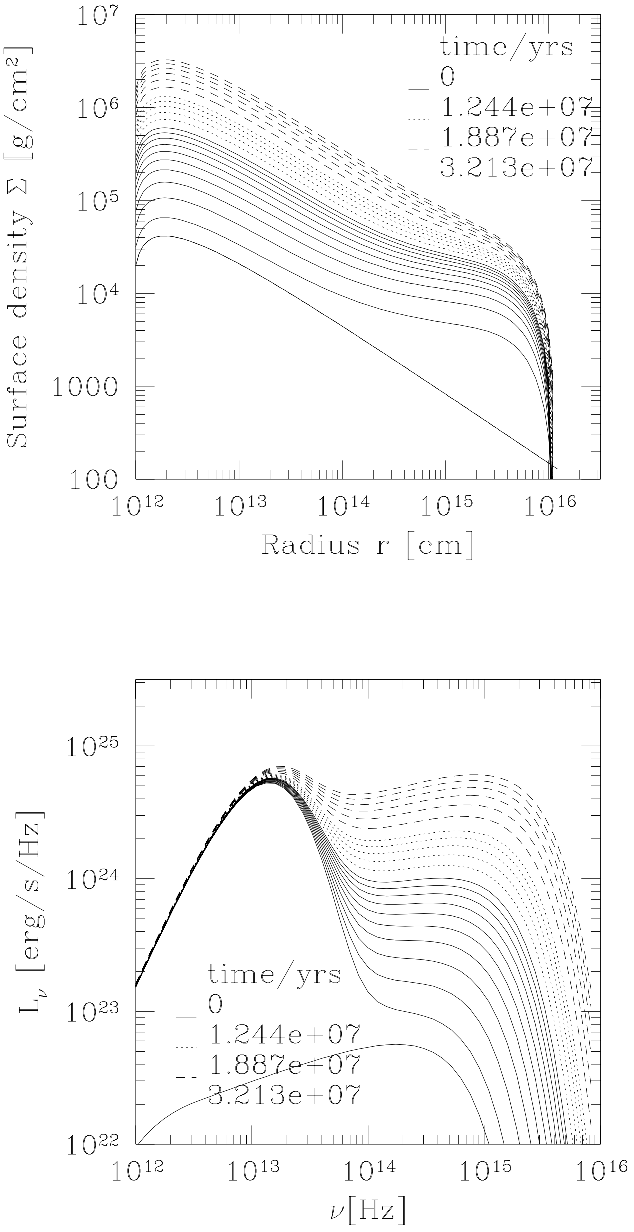

time/yrs
0
1.244e+07
1.887e+07
3.213e+07
Surface density Σ [g/cm²]
Radius r [cm]
time/yrs
0
1.244e+07
1.887e+07
3.213e+07
L_ν [erg/s/Hz]
ν[Hz]

Figure 5

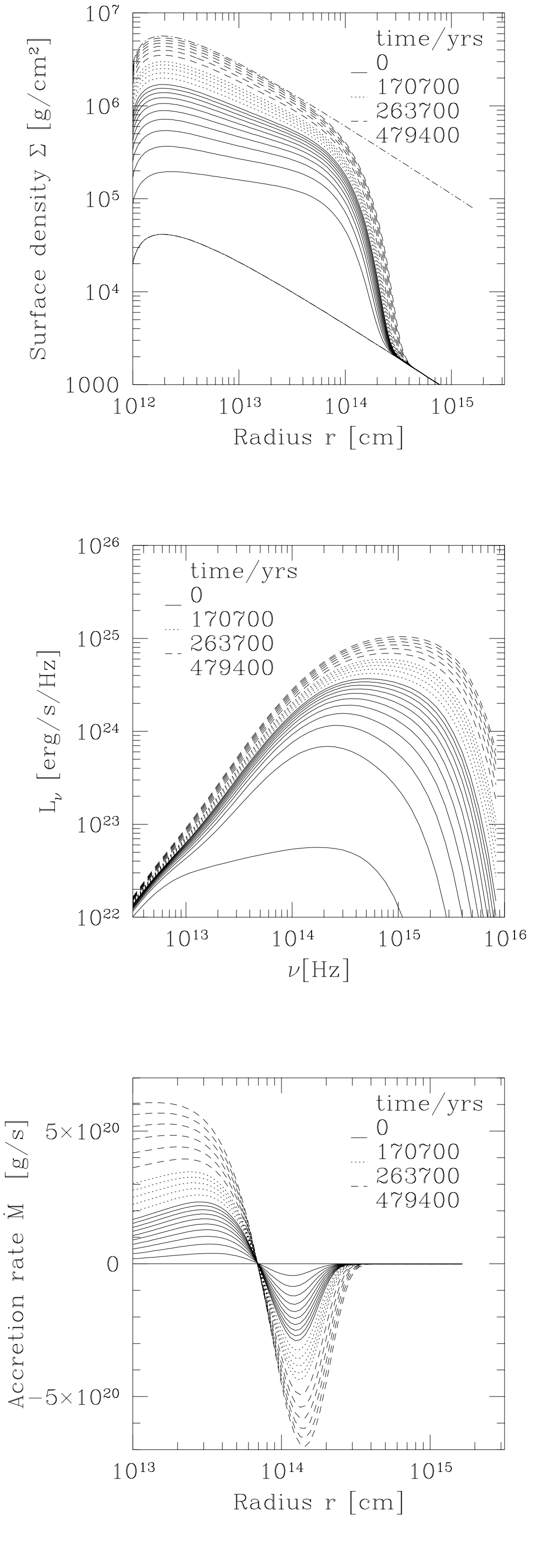

time/yrs
0
170700
263700
479400
Surface density Σ [g/cm²]
Radius r [cm]
time/yrs
0
170700
263700
479400
L_ν [erg/s/Hz]
ν[Hz]
time/yrs
0
170700
263700
479400
Accretion rate $\dot{M}$ [g/s]
Radius r [cm]

Figure 6

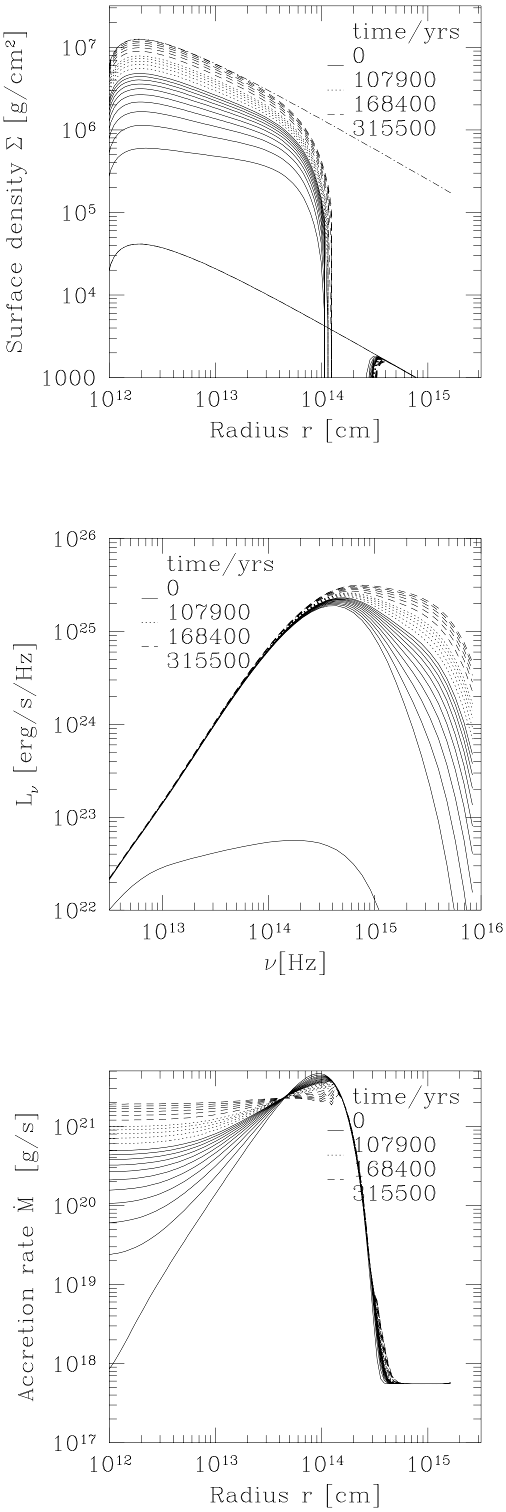
Surface density Σ [g/cm²]
Radius r [cm]
time/yrs
0
107900
168400
315500
L_ν [erg/s/Hz]
ν[Hz]
time/yrs
0
107900
168400
315500
Accretion rate $\dot{M}$ [g/s]
Radius r [cm]
time/yrs
0
107900
168400
315500

Figure 7